


Article

Simulation and Application of a New Multiphase Flow Ablation Test System for Thermal Protection Materials Based on Liquid Rocket Engine

Qingdong Su ^{1,2} , Bailin Zha ^{3,*}, Jinjin Wang ¹, Mingxia Yan ^{1,2}, Yong Gao ¹, Zhensheng Sun ¹ and Weifeng Huang ²

¹ Missile Engineering College, Rocket Force University of Engineering, Xi'an 710025, China

² Department of Mechanical Engineering, Tsinghua University, Beijing 100084, China

³ PLA Rocket Force Equipment Department, Project Management Center, Beijing 100085, China

* Correspondence: zhabailin@163.com

Abstract: Internal flow field ablation is an important issue in thermal protection materials for rocket engines and hypersonic vehicles. In this paper, a new multiphase flow ablation test system, with an Al₂O₃ particle delivery device based on an oxygen-kerosene liquid rocket engine, is designed and manufactured. A general variable-precision modular system simulation method is proposed to analyze the dynamic characteristics of the system. In addition, a unique internal flow field ablation test was performed on the 4D C/C composite simulating the working conditions of the SRM. The results show that the system can provide a wide temperature range (756~3565 K) and pressure range (0.2~4.2 MPa). The multi-disciplinary dynamic variable-precision system simulation method is helpful for more accurate design and test analysis, and the maximum error is less than 5%. The ablation tests show that the line ablation rate of the C/C composite nozzle at 3380 K and 1 MPa is 0.053 mm/s, verifying the combined effect of thermochemical and mechanical ablation. The ablation environment is controllable, which provides an effective way for the ablation test of thermal protection materials. In addition, the variable-precision dynamic simulation method has important reference value for the system design related to liquid rocket engine.

Keywords: liquid rocket engine; ablation; 4D C/C composite; internal flow field; multiphase flow; variable-precision system simulation



Citation: Su, Q.; Zha, B.; Wang, J.; Yan, M.; Gao, Y.; Sun, Z.; Huang, W. Simulation and Application of a New Multiphase Flow Ablation Test System for Thermal Protection Materials Based on Liquid Rocket Engine. *Aerospace* **2022**, *9*, 701. <https://doi.org/10.3390/aerospace9110701>

Academic Editor: Carmine Carmicino

Received: 27 September 2022

Accepted: 8 November 2022

Published: 9 November 2022

Publisher's Note: MDPI stays neutral with regard to jurisdictional claims in published maps and institutional affiliations.



Copyright: © 2022 by the authors. Licensee MDPI, Basel, Switzerland. This article is an open access article distributed under the terms and conditions of the Creative Commons Attribution (CC BY) license (<https://creativecommons.org/licenses/by/4.0/>).

1. Introduction

The air-breathing hypersonic vehicle (AHV), solid rocket motor (SRM) and solid rocket ramjet (SRR) experience severe thermochemical ablation and particle erosion during their operation. The ambient temperature of the thermal protection components in the nozzles, nose tips, or sharp leading edges are as high as 2000 °C or more, accompanied by complex oxidation and particle erosion [1–4]. In recent years, with the improvement of flight performance, thermal protection materials are facing more severe challenges.

C/C composites are widely used as thermal protection materials for ultra-high temperature due to their low density, high strength, and excellent mechanical properties at high temperature [5]; therefore, they are widely used as thermal protection materials for ultra-high temperature. The preparation and characterization of C/C composites with different processes and modification methods have advanced the research topic [6,7]. For the characterization of C/C composites ablation performance, there have been many experimental methods. It should be noted that the actual flight test is expensive, and the simple numerical simulations of complex ablation phenomena are often inaccurate due to the lack of real parameters of the material. Therefore, the equivalent thermal ablation test method under laboratory conditions has been widely studied and applied. The main methods are the oxyacetylene ablation test [8], the plasma ablation test [9,10], the model SRM

test [11], the model liquid rocket engine (LRE) ablation test [12,13], the laser ablation [14], the wind tunnel test [15], and the thermogravimetric analysis method [16], etc. For example, Fu et al. [8] studied the ablation behavior of C/C composites with one-shaped holes by an oxyacetylene flame, and found that under the heat flux of 4.18 MW/m^2 , C/C composites has a better ablation resistance than C/C-ZrC-SiC material. B. Helber et al. [9] used VKI Plasmatron to test carbon fibers under different combustion pressure environments, and found that the jet velocity increased in the low-pressure environment, leading to more obvious oxidation ablation. Chen et al. [10] used a plasma torch to study the effect of Cu additives on the improvement of the ablation resistance of C/C composites. The results showed that the ablation was more serious after the depletion of Cu additives. In addition, He et al. [11] designed a new small SRM to test the thermal insulation materials in the SRR, and obtained accurate ablation prediction results by the erosion simulation model. Based on a small oxygen-kerosene LRE, Zha et al. [12] constructed a supersonic ablation condition, and obtained the ablation mechanism of C/C-SiC and C/C-SiC-ZrC composites in an oxygen-enriched environment. Wei and Haidn et al. [13] analyzed the combustion and boundary thermal properties of a GOX/kerosene rocket engine, demonstrating the excellent properties of this type of combustion device. However, most of the ablation test methods mentioned above have varying limitations on the cost and flexibility in parameter adjustment. Taking the nozzle throat of the SRM as an example, the erosion effect of particles in the multiphase flow ablation environment is obvious, and the ablation results of pure high temperature gas flow have large errors compared with the actual conditions. Therefore, aiming at the ablation problem of the C/C composite material in the nozzle throat of the SRM, an internal multiphase flow ablation test system based on the LRE and a particle delivery device is designed, which has the advantage of a wide range of adjustable parameters.

It is obvious that the design and parameter settings of the multiphase flow ablation test system, which directly determine the ablation results, are seriously affected by the dynamic characteristics of the LRE system. Moreover, it is expensive and time-consuming to directly adjust the design of the experiment accompanied by a lot of trial and error, and some accurate parameters cannot be measured directly. To study the parameter design and adjustment process in detail, it is necessary to conduct a comprehensive system dynamic simulation, which is similar to the study of the system dynamic characteristics and control scheme in LRE engineering development [17,18]. In early research on the LRE, some basic ordinary differential equations make up the special programs [19,20]. Unfortunately, these codes (summarized as 'one machine, one program') closely related to the engine structure cannot meet the requirements of rapid tasks on complex system simulation. With the development of software engineering technology, research on general simulation programs have become the main direction, and the dimensions of simulation tasks have begun to develop from 0D to 3D. Some representative achievements are: German DRL Company's Modular Engine Analysis System [21]; NASA's ROCETS and its improved software ESAY5x [22]; France's CARINS [23]; Spain's EAI Company's Ecosim Pro; and the European Space Agency's ESPSS [24]. The National University of Defense Technology [25], Beihang University [26], and the general Xi'an Institute of Aerospace Propulsion [27] developed some general performance simulation software based on the Matlab simulink platform. In addition, a new software, Mworks [28], based on the Modelica language, was developed recently. Among the many common platforms, AMESim from Siemens, Germany, has some unique advantages, and there are SSME and RL-10A models in its liquid propulsion library [29]. Based on the AMESim platform, Li et al. [30] and Zheng et al. [31] conducted some studies on the dynamic characteristics of the expansion cycle LOX/methane engine. Liu et al. [32] and Li et al. [33] carried out systematic modeling of the electric pump LOX/kerosene engine, which confirmed the reliability of the method. The general modular modeling methods based on the AMESim platform significantly improves efficiency of engineering development.

In this paper, a new internal multiphase flow ablation test system based on a GOX/kerosene LRE is invented, where Al_2O_3 particles are used to model condensed-phase particles. Based on the AMESim platform, the pipelines, pumps, valves, thermal components, and control strategies, of the system are modeled by the modular simulation method and the automatic variable precision simulation method. By analyzing the dynamic characteristics of the system in detail, the experimental conditions satisfying the ablation environment are derived. In order to verify the reliability and feasibility of the method, the actual ablation/erosion test of C/C composites is carried out in the internal flow field containing the Al_2O_3 particles, and the ablation rate, morphology, and ablation mechanism of the material are analyzed.

2. Design and Simulation Method of the System

2.1. System Design and Composition

The internal multiphase flow ablation test system containing a unique particle conveyor is based on the ground test device of the electric GOX/kerosene LRE. As shown in Figure 1, the subassemblies of the ablation system include the combustion chamber, test bench, control center, high-pressure kerosene supply system, gas supply system, and cooling system.

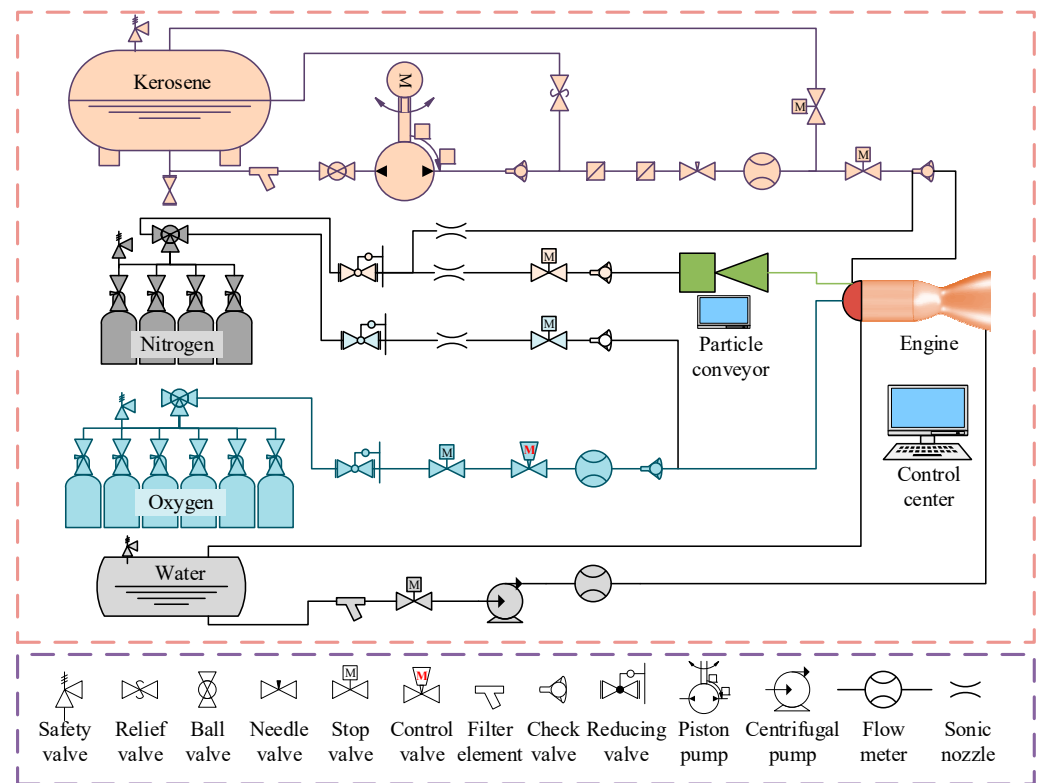


Figure 1. Structure of the ablation test system based on the GOX/kerosene LRE.

The kerosene is pressurized by the electric swashplate piston pump, and enters the injectors through the main valve and the check valve. The closed-loop control of kerosene flow is based on the speed regulation of variable frequency pump. The cooling unit adopts an air-cooled heat exchanger to keep a constant low temperature of the cooling water source. The water is pressurized by an external centrifugal pump and enters the heat exchange channel of the combustion chamber, and finally returns to the tank. The scheme of continuous circulation cooling meets the needs of long-term ablation tests.

As shown in Figure 2, a motor-driven rotary disk-type particle conveyor is used to add solid particles into the GOX/kerosene combustion chamber. Different from the simple mixing of particles in the jet in an open environment, the pressure-resistant design makes it

possible to directly inject solid-phase particles into the high-temperature and high-pressure gas in the internal flow field ablation test.

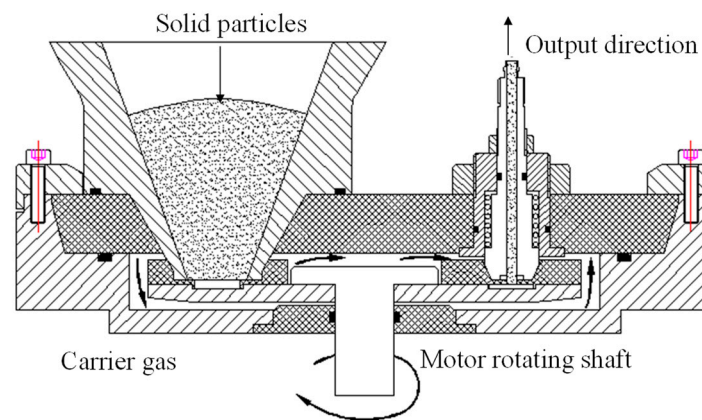


Figure 2. Structure of the solid particle conveyor.

The nitrogen system provides the purge gas for the aforementioned oxygen and kerosene propellant pipelines and a small amount of solid particle carrier gas. As an inert low temperature medium, nitrogen can also effectively change the ablation environment when the combustion temperature and speed are adjusted in a wide range. Most sensors are arranged in the control center, as well as some are in the kerosene hydraulic skid, power cabinet, thrust chamber, etc. The combustion chamber is made of copper material, and the cooling jacket is made up of milled grooves on the inner wall. The ignitor is a high-energy spark plug, which is installed in the head to provide energy (more than 10 J) to the repeated starts of the LRE.

The main technical metrics of engine are listed in Table 1. According to the requirements of the test tasks, the combustion chamber pressure is set to 1 MPa (gauge pressure), and the temperature is about 3380 K. Meanwhile, the diameter of the nozzle throat is 8 mm. According to the calculation of chemical equilibrium analysis (NASA CEA) program, a nominal mix ratio of 3.0 meets the combustion temperature requirements at the aforementioned pressure. As shown in Table 1, the ideal combustion stagnation temperature and characteristic velocity of the engine are 3456.67 K and 1735.7 m/s, respectively. Among them, the actual temperature is about 3380 K after the correction of the actual combustion efficiency. The propellant consumption flow under the current combustion conditions can be obtained by the following equation:

$$\dot{m} = P_c A_t / C^* \quad (1)$$

Table 1. Main ideal parameters of the combustion component.

Parameters	Symbol	Unit	Value
Combustion chamber pressure	P_c	MPa	1
Mixing ratio	μ		3.0
Throat diameter	D_t	mm	8
Total flow	\dot{m}	g/s	31.86
Oxygen flow	\dot{m}_o	g/s	23.895
Kerosene flow	\dot{m}_f	g/s	7.965
Nozzle exit diameter	D_e	mm	12
Combustion chamber diameter	D_c	mm	46
Combustion chamber length	L_c	mm	120

In the equation P_c is the absolute pressure of the combustion chamber (Pa), A_t is the throat area (m^2), and C^* is the characteristic velocity of combustion (m/s).

According to the characteristic length (L^*) and relative flow density (r_s^-) [34], the geometric parameters such as the volume and diameter of the combustion chamber are obtained. These parameters constitute the minimum constraints on the structural dimensions of the combustion chamber:

$$V_c = L^* A_t = L_c A_c \quad (2)$$

$$D_c = \sqrt{\frac{4A_c}{\pi}} = \sqrt{\frac{4}{\pi} \frac{\dot{m}}{r_s^-}} \quad (3)$$

The multiphase flow internal ablation test engine is shown in Figure 3, and its basic structure is a water-cooled GOX/kerosene rocket engine. The head adopts a gas-liquid coaxial orifice-swirl injector, the oxygen enters through the central straight hole, the kerosene fills the outside wall, then tangentially rotates into the mainstream through radially inclined holes, and atomized by the high-speed oxygen flow. Solid particles enter the combustion chamber from the head, creating the multiphase flow whose particle concentration is adjustable. The coolant flows downstream into the cooling jacket to cool the reusable combustion chamber. The specimen at the end of the combustion chamber is single-use, and its cooling form depends on itself. The material is consistent with that used in the actual SRM. The internal profile of the specimen is scaled down (30:1) according to the nozzle structure of the real engine.

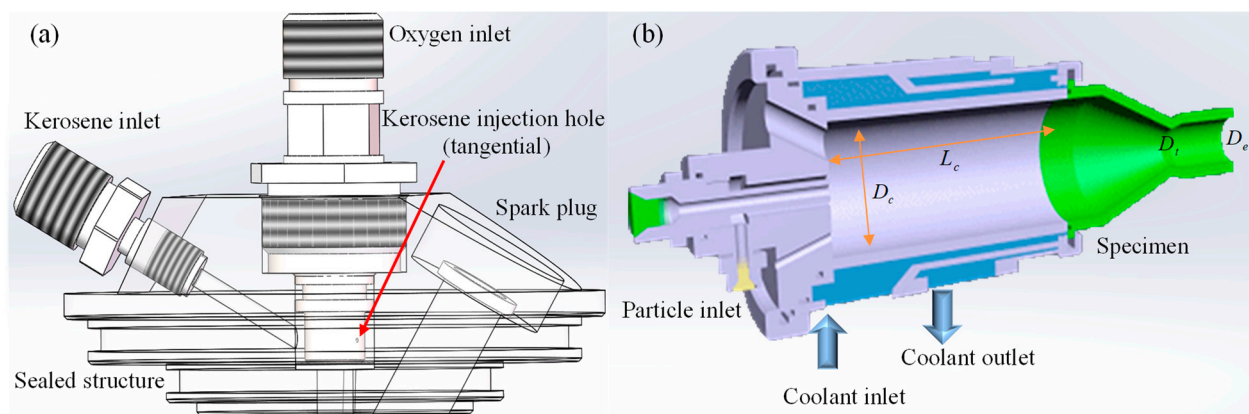


Figure 3. Structural of the multiphase flow internal ablation test engine. (a) Combustion chamber head; (b) Engine and specimen.

CEA calculations show that, including unreacted components, the combustion process will produce about a dozen products. The main components of combustion product are shown in Table 2.

Table 2. Main combustion product components.

Components	Mole Fraction
H ₂ O	0.28935
CO	0.26934
CO ₂	0.15681
OH	0.09147
H ₂	0.06050
O ₂	0.06009
H	0.03971
O	0.03260

2.2. Working Process

The ignition sequence is designed as Figure 4. Firstly, the cooling system is opened to fill the cooling jacket of the combustion chamber. Then, the high-pressure oxygen first

enters the combustion chamber and mixes with the sub-sequent kerosene, which facilitates the atomization of the fuel. The spark plug ignites the gas and liquid droplets mixture. When the system is shut down, kerosene is turned off first, and then oxygen, which avoids the backflow of high-pressure and high-temperature gas into the oxygen supply pipeline to burn the test device. The process needs to be very short in order to avoid the over-oxidation of the specimen as much as possible.

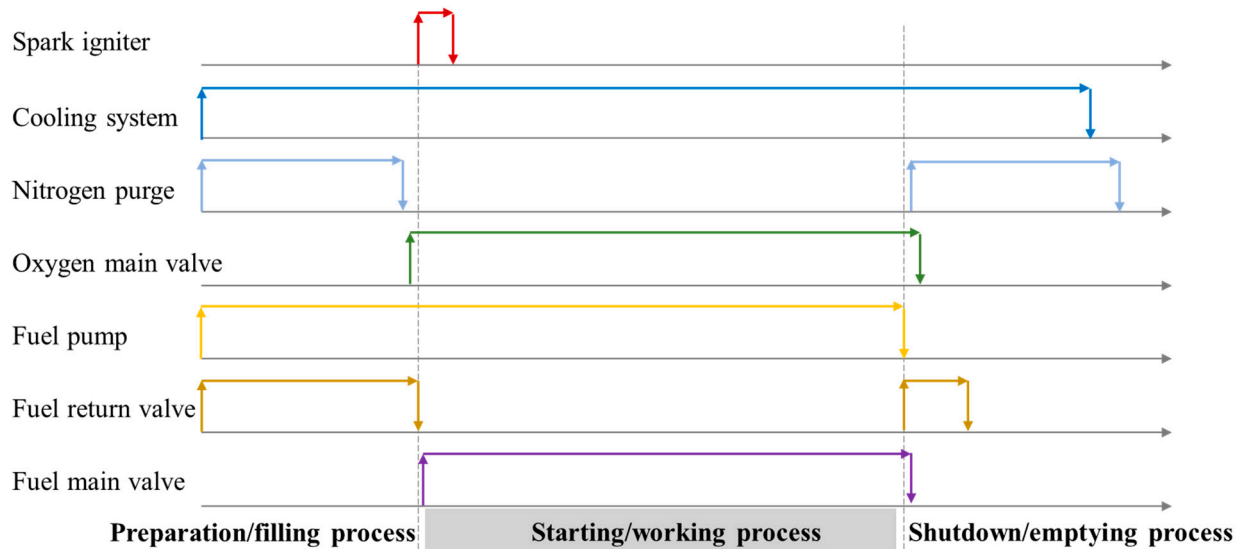


Figure 4. The ignition sequence of the GOX/kerosene LRE.

Before the test, the pipeline and engine cavity shall be purged with high pressure nitrogen. The preset parameters such as the pressure and flow of each node can be automatically adjusted by the control center. During the preparation stage, the kerosene return circuit complete the filling of the pipeline before the main valve, which improves the response speed of the fuel circuit. Furthermore, since the flow resistance of the return circuit can be adjusted to be consistent with the injector pipeline, the aforementioned self-circulation process facilitates the control and confirmation of the initial kerosene flow during ignition process.

When the system stops, the fuel pump is first closed, the return valve is opened at the same time, and the main fuel valve is closed. After a short delay, the main oxygen valve is closed and the nitrogen purge valve is opened for line purge. Finally, the cooling system is closed, the gas cylinder group is closed, and all pipelines containing high-pressure media are evacuated.

It should be noted that it is not possible to directly control the temperature and speed of the combustion chamber. The actual control parameters are the flow rate and the action time of the valves. Literature [35] indicates that the LRE parameters or ablation environment can be controlled more precisely with the help of a detailed model of the system characteristics.

2.3. System Simulation Model

It is necessary to study the dynamic characteristics of the GOX/kerosene ablation test system in order to give the component parameters for actual engineering implementation, and to determine the potential range of test conditions. A series of detailed dynamic system models are established based on the IRC method [30,36], including the pipelines, thermal components, pumps, and valves model. Moreover, the 0D/1D simulation models of the above components constitute a complete system. The simulation is carried out based on the AMESim platform.

2.3.1. Pipeline Numerical Model

Most system simulation typically focus on the parameters at low frequencies, and the main propellant and coolant pipeline elements can be divided into C, IR, or R cells [30,37]. These elements have capacitive, inertial, and resistive properties, respectively.

As for the liquid pipelines, the models are built on the AMESim thermal-hydraulic library [38], which is based on a transient heat transfer approach. The equations of pipeline pressure and temperature considering the heat exchange are:

$$\frac{dp}{dt} = \beta_{\text{eff}} \left[\frac{1}{\rho} \frac{d\rho}{dt} + \alpha \frac{dT}{dt} \right] \quad (4)$$

$$\frac{dT}{dt} = \frac{dh_{in} + \sum dm h_i - h \sum dm_i}{c_p \cdot \rho \cdot V_{\text{eff}}} + \frac{\alpha \cdot T}{c_p \cdot \rho} \frac{dp}{dt} \quad (5)$$

where ρ is the density, $\sum dm_i$ is the total input mass flow, $\sum dm h_i$ is the input total enthalpy, β_{eff} is the combined bulk modulus, V_{eff} is the effective volume, dh_{in} is the heat exchange between the pipeline and the outside.

The equivalent bulk modulus, which takes into account the elasticity of the fluid and the pipe wall, is expressed as:

$$\beta_{\text{eff}} = \left(\frac{1}{\beta_{\text{fluid}}} + \frac{w_{\text{comp}}}{1 + w_{\text{comp}} \cdot (p - p_0)} \right)^{-1} \quad (6)$$

In the equation β_{fluid} is the fluid elastic modulus that changes with temperature. w_{comp} is the compliance parameter of pipeline wall, and its value is the reciprocal of the elastic modulus β_{wall} . p_0 is the reference pressure.

The effective volume of the pipeline in Equation (5) is:

$$V_{\text{eff}} = V \cdot [1 + w_{\text{comp}} \cdot (p - p_0)] \quad (7)$$

Heat exchange of the pipeline is a function of heat exchange coefficient k_{th} , pipeline diameter D , pipeline length l_e , and temperature difference:

$$dh_{in} = k_{th} \cdot \pi \cdot D \cdot l_e \cdot (T_{ex} - T) \quad (8)$$

For a long pipeline, considering its frequency response and fluid inertia, the flow derivative is corrected by the friction term corresponding to the frequency. The flow derivative is:

$$\frac{\partial Q}{\partial t} = \frac{A}{\rho} \frac{\partial P}{\partial x} - g \cdot A \cdot \sin(\theta) - \frac{ff \cdot Q^2 \cdot \text{sign}(Q)}{2 \cdot D \cdot A} \quad (9)$$

where A is the cross-sectional area, which is a function of pressure in the elastic state. θ is the inclination angle between the pipeline and the horizontal plane, ff is the coefficient of friction.

The gas pipeline model references the pneumatic library of the AMESim [39]. The gas cylinder group is considered as a C unit, and the pipeline is considered as a C unit or a C-R unit. The governing equations obey the gas law and the laws of thermodynamics.

2.3.2. Thermal Components Model

The main thermal components include injectors, combustion chamber, nozzle, and cooling jacket. The injector is mainly composed of a cavity and a nozzle, which can be regarded as a combination of a C unit (cavity) and a R unit (nozzle). For a liquid injector, the mass flow \dot{m} is:

$$\dot{m} = \rho \cdot c_q \cdot A \cdot \sqrt{\frac{2 \cdot |\Delta P|}{\rho}} \quad (10)$$

where c_q is the flow coefficient, and A is the cross-sectional area of orifice. If c_q is a constant, the above equation has an infinite gradient at the origin, so the numerical model format needs to be improved as follows:

$$\lambda = \frac{D_h}{\nu} \cdot \sqrt{\frac{2|\Delta P|}{\rho}} \quad (11)$$

$$c_q = c_{qmax} \cdot \tanh\left(\frac{2\lambda}{\lambda_{crit}}\right) \quad (12)$$

where λ is the flow parameter, ν is the kinematic viscosity and c_{qmax} is a constant, the c_q varies approximately linearly with ΔP . The fluid Reynolds number is $Re = c_q \cdot \lambda$.

The model uses upstream parameters, so the enthalpy flow is:

$$dmh = \dot{m} \cdot h(P_{up}, T_{up}) \quad (13)$$

For the gas injector, the mass flow rate is [39]:

$$\dot{m} = C_q \cdot A \cdot \Psi \cdot \sqrt{\frac{2 \cdot P_{up} \cdot \rho_{up}}{k_{dp}}} \quad (14)$$

where k_{dp} is the pressure loss coefficient and Ψ is the flow function.

When the nozzle is not clogged, Ψ leads the Equation (14) to Equation (10). When clogged, it is a one-dimensional compressible flow, and Ψ is related to the pressure ratio:

$$\Psi = \begin{cases} \sqrt{\frac{1}{1-\gamma_s}} \cdot \sqrt{\eta^{2\gamma_s} - \eta^{1+\gamma_s}} & \eta > \eta_{cr} \\ \sqrt{\frac{\gamma_s}{1+\gamma_s}} \cdot \left(\frac{2\gamma_s}{\gamma_s+1}\right)^{\frac{\gamma_s}{1-\gamma_s}} & \eta \leq \eta_{cr} \end{cases} \quad (15)$$

In the equation γ_s is the isentropic heat factor in non-ideal gas state, η is the current pressure ratio, and η_{cr} is the critical pressure ratio.

The combustion chamber adopts a zero-dimensional premixed combustion model with fixed delay [35,36]. The model is based on the assumptions of adiabatic, homogeneous, and ignoring liquid volume, and finally an executable simulation model is built on the AMESim signal library [40] and the gas mixture library [41].

The mixed gas in the combustion chamber conforms to the law of mass conservation:

$$\frac{dm_c}{dt} = \dot{m}_o(t - \tau) + \dot{m}_f(t - \tau) - \dot{m}_{out} \quad (16)$$

$$\frac{d\rho}{dt} = \frac{1}{V_c} \cdot \frac{dm_c}{dt} \quad (17)$$

In the equation τ is the time delay parameter, V_c is the volume of the combustion chamber. According to the state equation of ideal gas, the mixing ratio is:

$$\frac{dK}{dt} = (1 + K) \left(dm_o - K \times dm_f \right) \cdot \frac{RT}{P_c V_c} \quad (18)$$

In the equation dm_o and dm_f are the mass flow of oxidant and fuel, respectively.

There are 10 main reactants and products involved in the combustion reaction simulation, such as CO, CO₂, H₂O, etc. A multi-dimension thermodynamics database is generated by a self-developed Matlab and CEA coupling automatic program, and the interpolation covers the pressure range of 0~10 MPa and the mixing ratio of 0~500. As a result, the mass

fraction of each component and the temperature of the mixture can be quickly calculated, and the calorific value of the gas RT can be obtained:

$$RT = RT(K, P_c) \tag{19}$$

As a mixture gas cavity, the dynamic equation of the chamber pressure is:

$$\frac{dP_c}{dt} = \frac{RT}{V_c} \cdot \frac{dm_c}{dt} + \frac{P_c}{RT} \cdot \frac{d(RT)}{dt} - \frac{P_c}{V_c} \cdot \frac{dV_c}{dt} \tag{20}$$

Since the AMESim software does not have the reaction of RP-1 with oxygen, the customized combustion chamber simulation model is designed as a super component, as shown in Figure 5, which is an efficient graphical modeling method.

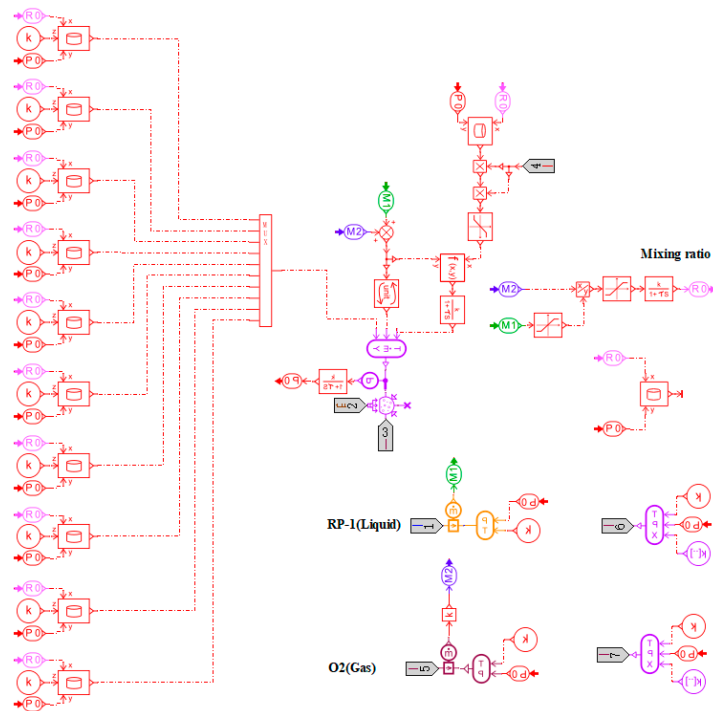


Figure 5. Custom simulation model of the combustion chamber.

The nozzle is the key component to convert the combustion energy into mechanical energy, and it accelerates the gas flow and generates thrust. Unlike the traditional LRE system simulation tasks, the ablation test system simulation does not focus on analyzing the thrust. However, the nozzle is the main structure of the specimen, and its model has an important influence on the calculation of the combustion chamber governing equations. The outlet of the combustion chamber is directly connected to the nozzle, so the flow out of the combustion chamber is equal to that of the nozzle \dot{m}_{nozzle} . Considering the real gas effect and energy loss, the calculation equation of nozzle flow under the assumption of frozen flow is:

$$\dot{m}_{nozzle} = A_t \cdot C_q \cdot C_m \cdot \frac{p_{up}}{\sqrt{T_{up}}} \tag{21}$$

The upstream parameters are used in the equation. When the loss of total pressure and total temperature are not considered, p_{up} and T_{up} are equivalent to P_c and T in the combustion chamber, respectively. The enthalpy flow is the same as Equation (14), and C_m is the nozzle’s flow parameter:

$$C_m = \sqrt{\frac{2\rho_{up} \cdot T_{up}}{p_{up}}} \Psi \tag{22}$$

The engine thrust considering the environmental pressure is:

$$F = \dot{m}_{nozzle} v_e + (p_e - p_a) A_e \quad (23)$$

In the equation v_e is the exhaust velocity.

$$v_e = \begin{cases} \sqrt{\frac{2}{1-\gamma_s} \cdot \frac{p_{up}}{\rho_{up}}} \cdot \sqrt{1 - \left(\frac{p_{dn}}{p_{up}}\right)^{1-\gamma_s}} & \eta > \eta_{cr} \\ \sqrt{\frac{2}{1+\gamma_s} \cdot \frac{p_{up}}{\rho_{up}}} & \eta \leq \eta_{cr} \end{cases} \quad (24)$$

The nozzle model also considers the gas separation of the one-dimensional jet. The separation position is calculated according to the nozzle flow separation standard in reference [42], which is beneficial to improve the calculation accuracy of velocity and thrust.

The calculation of heat exchange is based on the AMESim's thermal library [43] and thermohydraulic library [38]. As for the water-cooled jacket, the Bartz method [36] is adopted to calculate the heat transfer on the gas side, and the heat exchange model of jacket flow [33] is used to calculate the heat transfer between the wall and the coolant.

2.3.3. Pump Model

The liquid propellant flow is controlled by fixed orifices and pumps. There are two different pumps in the system: kerosene pump and coolant pump. The kerosene pump is a piston pump, and the numerical model based on the AMESim platform [38] takes into account factors such as fine components, mechanical inertia, and seal clearance. The volume flow is:

$$Q = -\frac{\Delta p}{12\mu l_c} r_c^3 \pi d_p \left(1 + \frac{3}{2} \left(\frac{ecc}{r_c}\right)^2\right) + \frac{v^+ + v^-}{2} r_c \pi d_p \quad (25)$$

where Δp is the pressure difference between the front and rear of the piston, r_c is the radial clearance, d_p is the outer diameter of the piston, l_c is the contact length, μ is the average hydrodynamic viscosity, ecc is the eccentricity of the piston, v^+ and v^- are the sleeve and piston speed, respectively.

There are special sealing structures such as sliding shoes and valve plates in the piston pump. The numerical model is:

$$\frac{dp_{ni}}{dt} = \frac{\beta \cdot (-Q - \sum dvol_i)}{(v_0 + \sum vol_i)} + \beta \alpha \frac{dT_{ni}}{dt} \quad (26)$$

$$Q = Q_{nini} + Q_{nouti} + Q_{nlspi} + Q_{nlpci} + Q_{nlbpp} \quad (27)$$

where the vol_i is the sum of the constant volume and the variable volume of each chamber. The pressure is determined by the total flow Q , which consists of the inlet flow Q_{nini} , the outlet flow Q_{nouti} , the external leakage flow Q_{nlspi} , Q_{nlpci} , and Q_{nlbpp} .

The cavity of the kerosene pump is variable, and its outlet and inlet flow are calculated by the orifice flow in Equation (10). There are three external leakage channels, which consists of piston-cylinder, swash plate-slipper and sleeve-distribution plate. The average flow and efficiency are:

$$Q_{Th} = displ \times \omega \quad (28)$$

$$\eta_{vol} = \frac{Q_{mean}}{Q_{Th}} \quad (29)$$

In the equation $displ$ is the theoretical displacement of the pump and ω is the rotation speed.

Since the actual object of the speed control of the plunger pump is the motor driven by the inverter, an advanced Squirrel-Cage Induction Machine (SCIM) motor model is established based on the electrical basics library [44] and the electric motors and drives library [45]. The model of the electric motor and piston pump are shown in Figure 6.

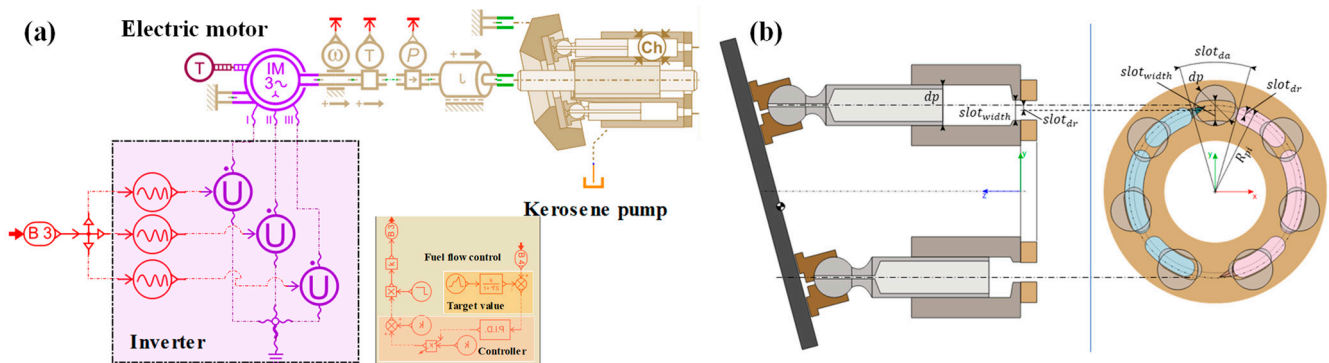


Figure 6. The sketch of electric piston pump. (a) AMESim model; (b) The basic structure.

The coolant pump is a centrifugal Suter pump [35,46], and its parameters are corrected according to the measured rated head, flow, rotational speed, and efficiency. The power of the coolant pump comes from a variable speed motor, which is a functional numerical model in the AMESim mechanical library.

2.3.4. Valve Model

Almost all valve models in the system can be equivalent to variable-section orifices, which are the same as Equations (10) and (14). The dynamic characteristics of the valve are fitted through the first-order time lag to meet the accuracy requirements.

2.3.5. CFD Coupled Model of the Combustion Chamber

The development process of combustion and gas jet in the ablation test can be analyzed in detail by the 0D/3D flow field coupled simulation model, based on the loosely coupled method. The simulation is performed on the AMESim and the Star CCM. The automatic calculation method, which does not rely on frequent manual modification and export of parameters between different software, makes a balance between the accuracy and efficiency of a complex system simulation.

Due to the axisymmetric structure of the combustion chamber, the simulation is performed only in the 7.2° region in the circumferential direction, and symmetry conditions are used at the boundary. Figure 7 shows the geometric boundary condition settings and meshing scheme, with a polyhedral mesh for the gas area. The boundary layer wall y^+ is between 30 and 200, and the final mesh count is about 960,000. The computational grid is generated by the Star CCM. The governing equations are discretized and solved by the finite volume method, and the coupling algorithm solves the coupling problem of velocity and pressure. The turbulent flow is simplified by the $k-\omega$ SST model, the convection term is discretized by the second-order upwind method, and the viscous term is discretized by the central difference method.

The inlet is the stagnation inlet, and the total pressure and total temperature come from the automatic output results of the 0D/1D system simulation model. The wall of the chamber is a non-slip adiabatic boundary with a fixed average temperature, and its temperature value is the same as the simulation result of the 0D/1D system. The outlet boundary is the pressure outlet, which is set to 0.1 MPa. The system transfers these parameters to the 3D numerical model via the TCP/IP protocol in a fixed time step.

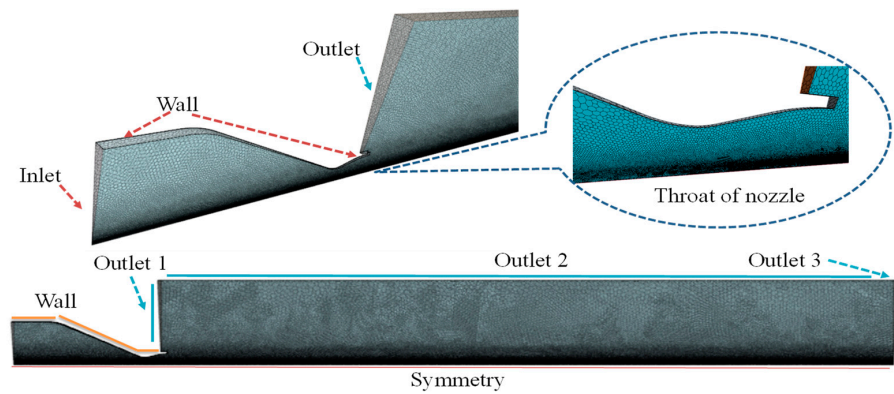


Figure 7. Geometric boundary condition settings and meshing scheme.

Combining the above component models, the overall system model is shown in the following Figure 8. In order to analyze the simulation results in combination with the test data, the corresponding relationship between the output parameters of the simulation model and the displayed parameters of the actual sensors is marked in the following figure, represented by “①~⑬”. The model has 144 variables and 144 dynamic equations, which is a simplification of the actual complex system structure. The equations are solved by the variable-step integral method, which has the advantages of faster solution speed and better stability.

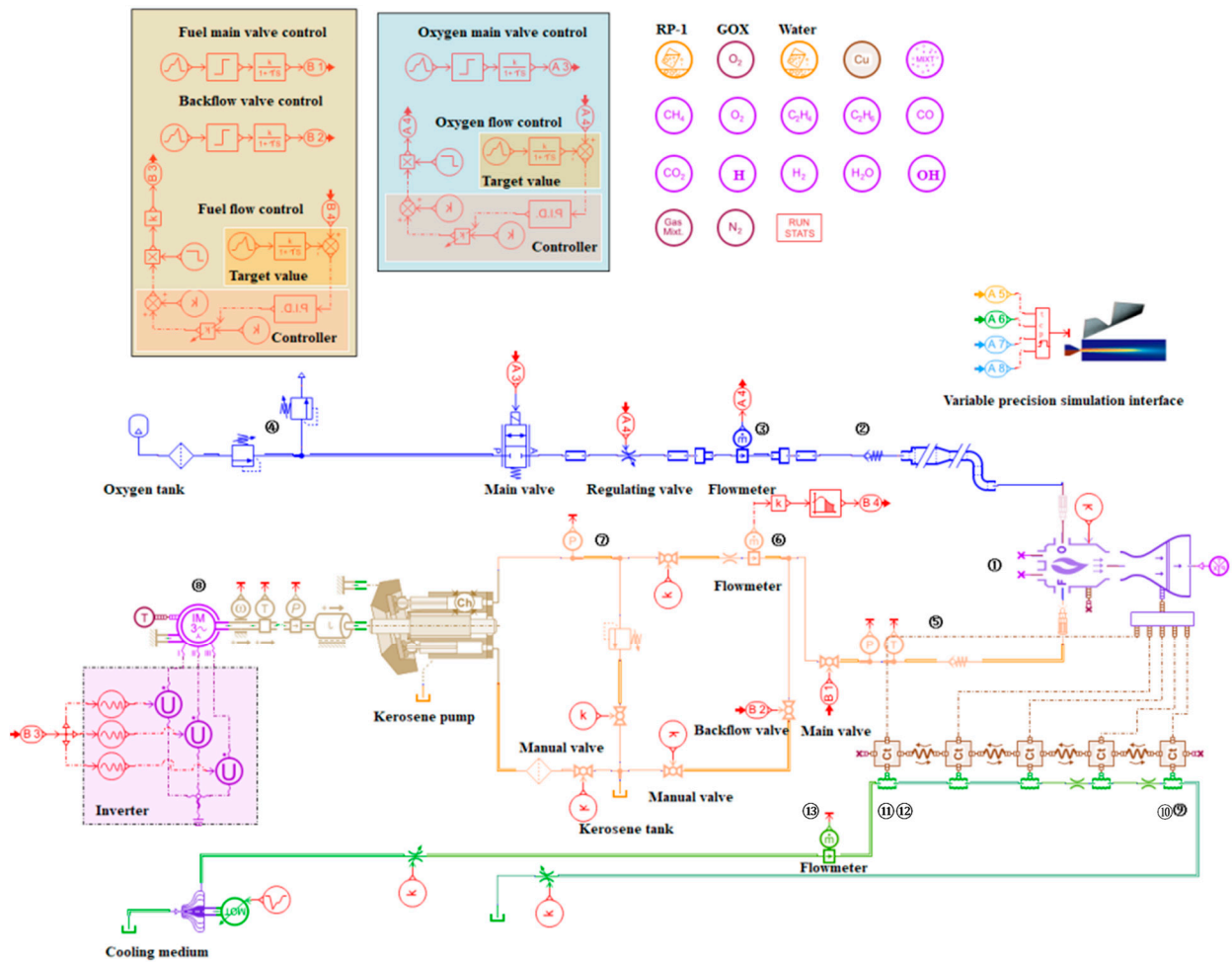


Figure 8. Graphical simulation model of the whole system dynamic characteristics.

Due to the good atomization of the gas-liquid coaxial atomizing injector, the system can work stably in a very wide mixing ratio and total flow range. According to the pipeline, valve size, and sensor ranges, the maximum flow that the system can provide is shown in Table 3. The table shows the temperature and pressure ranges that the ablation test system can cover (assuming the nozzle throat diameter is still 8 mm). These parameters are calculated based on the above numerical simulation model. Furthermore, the simulation shows that the temperature is greatly affected by the mixing ratio and is less affected by the pressure. The final temperature and pressure are determined by the mixing ratio and the total flow. If the throat area is adjusted or nitrogen is added in the combustion chamber, the parameter adjustment of the ablation environment can be more flexible.

Table 3. Main parameter range of the test system.

Parameters	Flow Range (g/s)	Pressure at Source (MPa)	Precision	Temperature (K)	Chamber Pressure (MPa)
Kerosene	2.00~29.47	6	1.5%	756~3565	0.2~4.2
Oxygen	7.15~95.27	6	1%		
Nitrogen	0~41.67	6	1%		
Coolant	833.33	2	1.5%		

The ablation test system based on a GOX/kerosene LRE engine has a large number of controllable parameters, of which temperature, velocity, and particle concentration are the most representative. They can be used as the main relevant parameters to re-produce the ablation environment. Similar relevant parameters are also used in the references [6,11,12]. The determination of these parameters mainly depends on the system simulation model (including 3D flow field simulation). In addition, the size of the particles needs to be similar to the diameter distribution of particles in the actual engine, and the internal profile of the specimen is similar to that of the actual SRM throat.

3. Experimental

3.1. Material Preparation

The ablation test object is the C/C composite used in the SRM. The main raw materials are carbon fiber, pultruded carbon fiber rigid rod, high temperature coal tar pitch impregnating agent. The 4D C/C composite in this study is braided by the shaft rod method, the carbon rods are arranged in parallel in the axial direction (Z direction), and the carbon fibers are woven in the carbon rod gap layer by layer in the X-Y plane according to $0^\circ/120^\circ/240^\circ$. The prefab density is 0.72 g/cm^3 . Then, the composites were prepared by the atmospheric pressure pitch impregnation carbonization (PIP) and high-pressure pitch impregnation carbonization (HPIP) process, and the final density is about 1.91 g/cm^3 .

The original material is finally machined into some nozzles, and the size is determined by the test requirements. Figure 9a shows the basic size of the specimen, whose boss structure is retained in order to make it more convenient to connect with the combustion chamber by screwing. The solid particles required for the multiphase flow ablation test are the Al_2O_3 powder, which is obtained by the sintering and crushing method. The particle size is $15\text{--}45 \mu\text{m}$, and the purity is higher than 99.4%. The selection of Al_2O_3 particles of this size and shape is mainly based on the measurement results of condensed particles after the actual rocket propellant combustion test, which is also similar to the reference value [11,47–49]. Figure 9b is the macroscopic and microscopic topography of the Al_2O_3 powder. The particles have a uniform particle size, good fluidity, and an irregular polygonal shape in the microscopic image. In addition, the ideal mechanical and thermodynamic properties of the C/C composite are provided, as shown in Figure 9c.

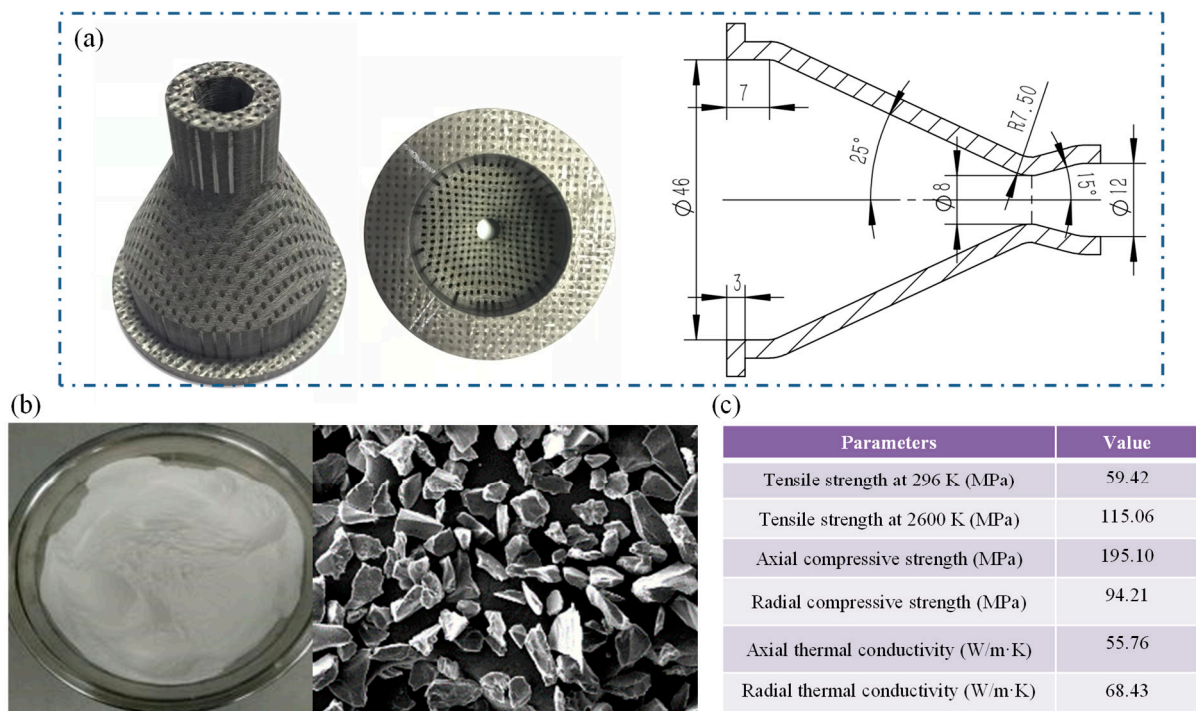


Figure 9. The morphology and main parameters of the specimen and the Al_2O_3 powder. (a) The specimen before ablation test; (b) Al_2O_3 powder and the SEM photograph; (c) Ideal properties of C/C composites.

3.2. Ablation System Deployment and Test Procedure

The ablation system built according to the design scheme is shown in Figure 10. Various devices are connected by pipelines and cables, and the oxygen and kerosene are stored separately. In order to control the flow of kerosene precisely, an integrated hydraulic station is designed. The particle conveyor is remotely operated by the control center, and the particles are fed into the combustion chamber by a trace amount of carrier gas. The actual control parameters are the test time, the flow of kerosene, and oxygen, which are realized by embedded control algorithm, human-machine interface (HMI) and electric actuator. The high resolution remote control camera (Canon EOS 70D, Ota Ward, Tokyo, Japan) is used to observe specimen and multiphase flow fields in the ablative tests. Temperature sensors (Meacon PT100, Hangzhou, China), pressure sensors (Microsensor MPM270, Baoji, China), gas flowmeters (Sevenstar D07, Beijing, China), and liquid flowmeters (Krohne Opimass 3400-S03, Duisburg, Germany), are deployed on the measuring nodes described in Figure 8 to obtain the detail parameters of the ablation system.

The ablation test process is shown in Figure 11, which mainly divided into six steps. First, the ideal conditions for the ablation test are determined according to the actual working conditions of the material. The preparation of the ablation specimen and associated test material is then completed. Considering that the temperature and velocity conditions are usually difficult to be directly measured and controlled in real time, it is necessary to design operable control parameters and analyze their accuracy. Then, install the specimen, prepare cameras, thermometers, and other necessary observation equipment. The system supports automatic startup, shutdown, and automatic data collection. Finally, the results of the ablation test shall be analyzed. If the results are not satisfactory, it is necessary to analyze the reasons according to the system simulation results and measured parameters, return to the steps of parameter setting, and restart the test. It should be noted that the high-precision dynamic simulation model is helpful to analyze the characteristics of the ablation test system comprehensively and guide the parameter adjustment. The method of system simulation research has been widely applied in the real LRE project.

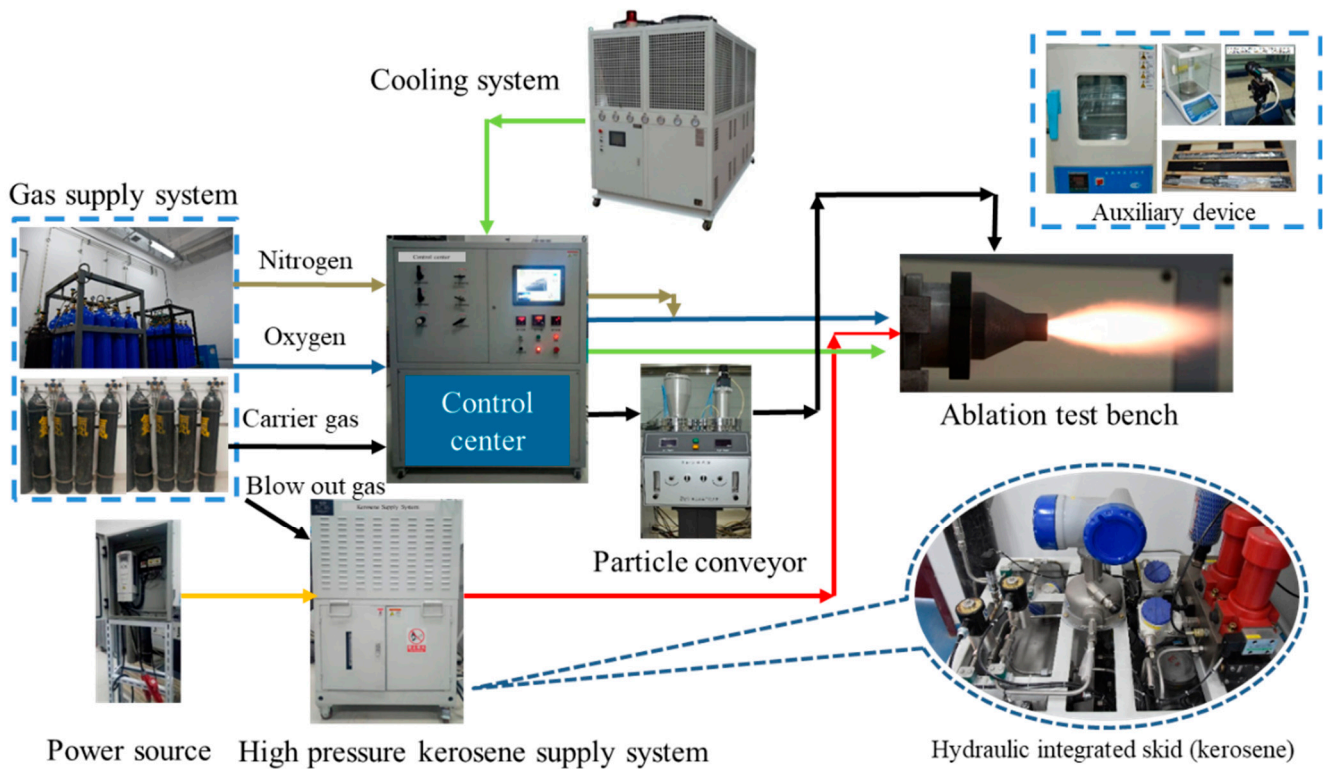


Figure 10. Experimental design of multiphase flow ablation based on liquid rocket engine system.

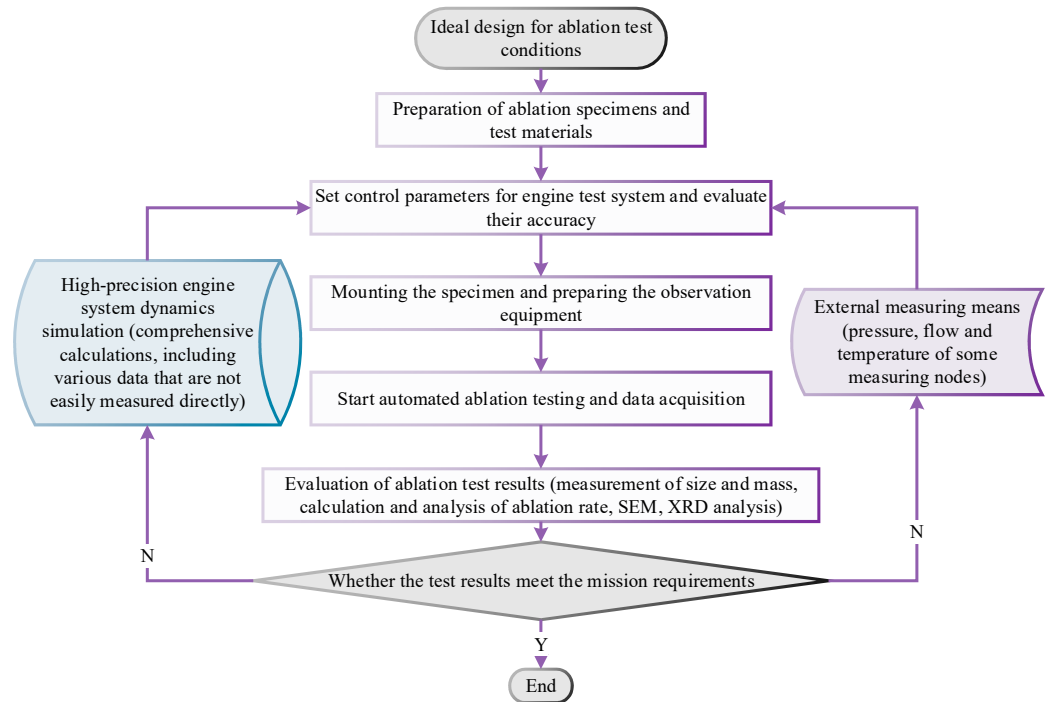


Figure 11. Procedure for ablation test.

Different from the ideal calculation results of the CEA program, the system simulation is carried out in the AMESim platform, and the final results considering the actual combustion efficiency have slight corrections. According to the requirements of the test task, the parameters of the specimens and the control parameters are shown in Table 4.

Table 4. Specimen parameters and control parameters of the ablation test.

Sample Number	Density (g/cm ³)	Kerosen (g/s)	Oxygen (g/s)	Ratio	Particle (wt.%)	Ablation Time (s)
1#	1.91	8.2	24.6	3.0	10	40
2#	1.89	8.2	24.6	3.0	10	40
3#	1.92	8.2	24.6	3.0	10	40

The calculation equation of particle concentration is:

$$\eta = \frac{G}{m_o + m_f + G} \quad (30)$$

G is the mass flow rate of particles, m_o is the mass flow rate of oxygen, m_f is the mass flow rate of kerosene, and the unit is unified as g/s.

3.3. Characterizations and Measurements

After the test, the ablation performance is evaluated by the line ablation rate and the mass ablation rate. A precision electronic balance is used to measure the quality of the specimen before and after ablation, and a precision depth gauge is used to measure the thickness of the specimen surface before and after ablation. The mass ablation rate (R_m) and the line ablation rate (R_d) are as follows:

$$R_m = (m_1 - m_2)/t \quad (31)$$

$$R_d = (d_1 - d_2)/t \quad (32)$$

where m_1 and d_1 is the mass (g) and thickness (mm) before ablation, m_2 and d_2 is the mass and thickness after ablation, and t is the effective ablation time.

The line ablation rate is measured by the high-energy X-ray micro CT (Bruker SKY-SCAN 1273, Karlsruhe, Germany). For each specimen, the plane containing the central axis of the specimen is scanned every 120°, and the change of 1D line segment length (diameter of throat) of the critical section of nozzle throat on the plane is taken as the calculation basis of line ablation rate. The final line ablation rate of the material is the average of the three specimens. Meanwhile, the mass of the specimen is measured by high precision electronic balance (Sartorius BSA623S, Gottingen, Germany), and the mass ablation rate is the value of the mass difference before and after the ablation tests. The final mass ablation rate of the material is the average of the three specimens. In addition, the microstructure of the composites is characterized by the scanning electron microscope (FEI Quanta 200 FEG, Hillsborough, OR, USA).

4. Results and Discussion

The simulation results of the startup and shutdown process of the multiphase flow ablation system based on the LRE are shown in Figure 12. At the initial stage, the combustion chamber temperature and mixing ratio rise rapidly without obvious pulsation shock. After that, the propellant mixing ratio is stabilized at 3.0, and the corresponding average temperature of the combustion chamber (the inlet of the ablated specimen) is fixed at 3380 K during the steady-state operation. In addition, Figure 12b shows that the system start-up filling time is about 0.66 s, and the transition time to establish a stable rated pressure after ignition is 0.42 s. In the steady state working stage, the flow rate of kerosene is 8.2 g/s, the flow rate of oxygen is 24.6 g/s, and the pressure of combustion chamber is 1.004 MPa (gauge pressure), in which the kerosene is pressurized by the swash plate plunger pump, resulting in a certain pulsation of the supply. Because of the system damping, inertia and combustion coupling, the main parameters of the combustion chamber have insignificant fluctuations (less than 2.2% of the average rated value). Furthermore, the simulation shows that the steady-state ablation test time is 39.64 s, which can be used as the time parameter

of the subsequent ablation rate calculation equation. In the shutdown stage, the pressure of the combustion chamber drops instantaneously due to the firstly turnoff of kerosene, and the reduction of the back pressure leads to a slight rise in oxygen flow in a short time, whose process lasts for about 0.54 s.

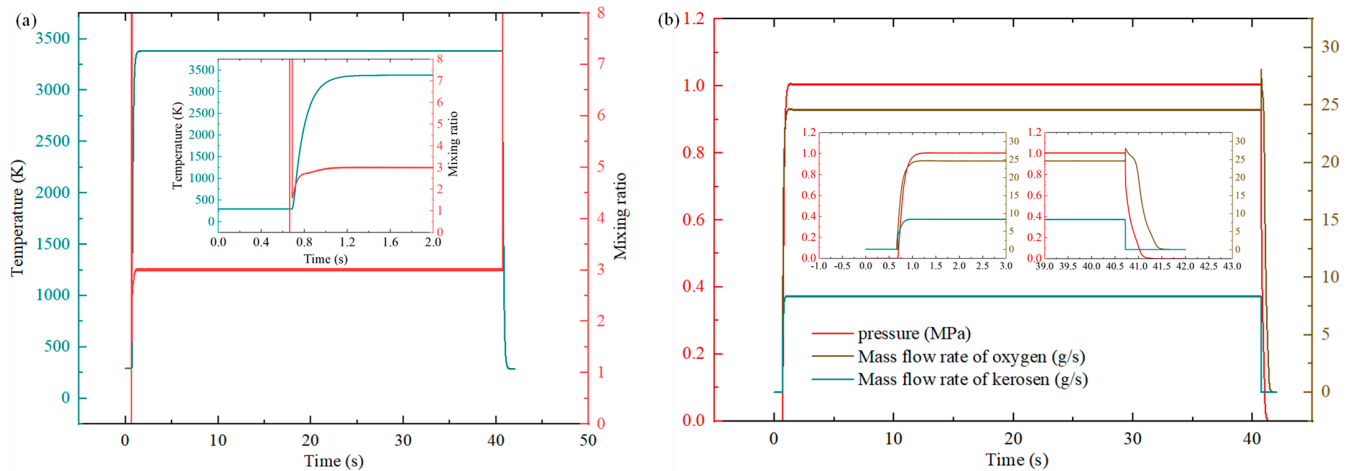


Figure 12. Start-up and shutdown process of the ablation test system over time. (a) Temperature and mixing ratio; (b) Chamber pressure and flow of propellants.

The system simulation gives the key parameters of all components in the working process, and the actual sensors of the test system at the 13 main nodes are shown in Figure 8. As a direct verification of the simulation results, the comparison of the simulated and measured parameters of each node in the steady state is shown in the Table 5. The first group (light blue) is the parameters of the oxygen supply circuit. When the control valve opening is 21%, the gas source pressure of 5.6 MPa ensures the stability of the gas flow during the test. The total pressure decreases as the gas passes through a series of components in the supply path, and the final pressure drop of the gas injector at the head of the combustion chamber is 0.57 MPa, which is conducive to stable combustion. The second group (light yellow) are the parameters of the kerosene supply circuit. When the frequency of the variable frequency controller of the kerosene pump is about 19 Hz, the kerosene enters the liquid injector in the head of the combustion chamber through the valve and the flowmeter, and the pressure drop of the injector is 0.5 MPa, which is also conducive to maintaining stable combustion. It is worth noting that due to the low liquid flow rate and the small pipeline flow resistance, the main pressure drop occurs at the kerosene injector. The third group (light green) are the parameters of the cooling water supply circuit. With the centrifugal pump operating at the rated point, the cooling water near the constant temperature enters the cooling jacket of the combustion chamber through the pipeline and the measuring element. The inlet pressure of the cooling water is 1.2 MPa, and the outlet pressure is close to the ambient pressure. The main throttling occurs in the cooling channel. These parameters ensure that the cooling medium at the heat exchange position has a higher pressure, and thus the combustion chamber has a sufficient convective heat exchange margin.

The heat exchange of the ablation test device mainly occurs on the heat exchange boundary, and the cooling method of the specimen in the internal ablation test is radiation cooling. In the system simulation, the heat exchange nodes are marked as ①~⑤, as shown in Figure 13. It shows the temperature change of the cooling medium at each thermal node, and the temperature of the cooling medium passing through the heat exchanger increases from about 10 °C to 43 °C. With the extension of the test time, the temperature has a slow upward trend. The water-cooled heat transfer results are consistent with the experimental measurements. In addition, the heat transfer model calculation shows that the maximum temperature of the gas side of the combustion chamber wall is 656 K, and the

average temperature of the material substrate is about 580 K, which is within the required temperature range of copper materials. Therefore, the water-cooled heat exchange effect of the reusable combustion chamber is as expected, and it can meet the needs of repeated ablation tests for a long time.

Table 5. Comparison of simulated and measured steady-state parameters of key nodes in the ablation test system.

NO.	Simulation Value	Sensor Value	NO.	Simulation Value	Sensor Value
1#	1.004 MPa	1.01 MPa	8#	18.95 Hz	19.75 Hz
2#	1.552 MPa	1.58 MPa	9#	43.92 °C	42.35 °C
3#	24.603 g/s	24.6 g/s	10#	0.029 MPa	0.04 MPa
4#	5.856 MPa	5.64 MPa	11#	9.57 °C	10.06 °C
5#	1.557 MPa	1.61 MPa	12#	1.145 MPa	1.21 MPa
6#	8.205 g/s	8.2 g/s	13#	609.257 g/s	620.4 g/s
7#	1.582 MPa	1.63 MPa			

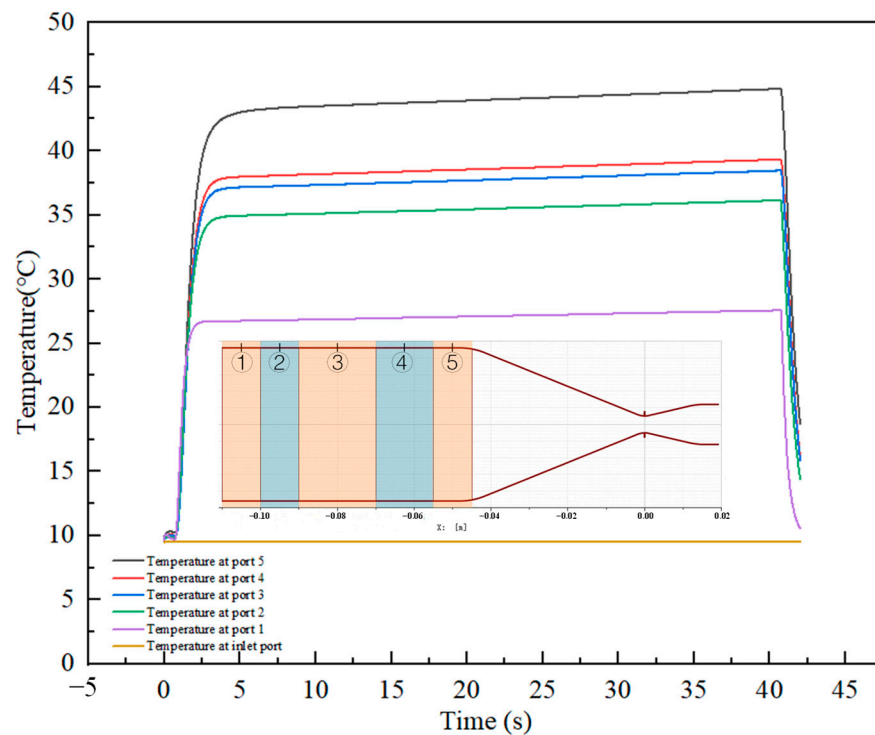


Figure 13. Thermal characteristics of the regenerative cooling medium of the ablation device.

The simulation results of the flow field are shown in Figure 14. A variable precision simulation method is to input the thermodynamic parameters (total gas pressure, total temperature, and molar mass, etc.) generated by the 0D and 1D system simulation into the 3D CFD simulation model through the TCP/IP data interface. Figure 14a shows the velocity, temperature, and static pressure changes along the axial direction of the specimen. On the one hand, the gas velocity rapidly increases to about 2400 m/s after accelerating in the expansion section of the Laval nozzle, then it fluctuates violently with a series of expansion and compression waves at the nozzle outlet, and finally decays gradually. On the other hand, the gas temperature drops rapidly from 3380 K to about 2000 K, showing an opposite trend to the gas velocity at the position where the shock wave generated (the conversion of momentum and energy occurred through the shock wave). In addition, the static gas pressure after the Laval nozzle outlet drops significantly, even lower than the ambient pressure, which directly explains the compression wave phenomenon caused by the over-expansion of the gas during the flow process. The flow field simulation gives the

internal environment of the ablation device, and the flow field structure is compared with the actual jet image, which shows that the simulation results are reliable.

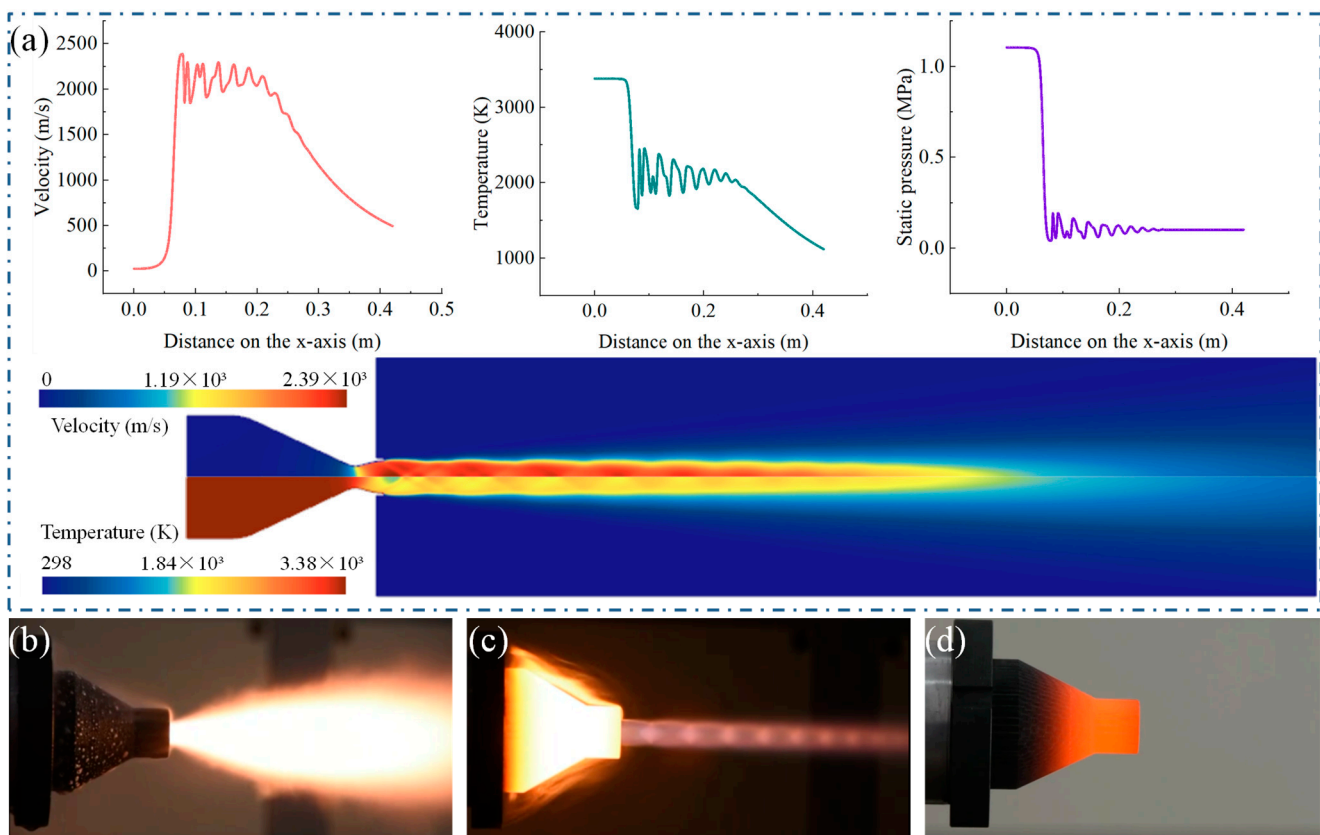
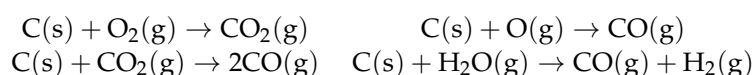


Figure 14. Steady-state flow parameters of combustion chamber and images of ablation test. (a) Combustion CFD flow field in stable working stage; (b) Ignition stage; (c) Stable working stage; (d) Shutdown stage.

Figure 14b–d are the stages of the ablation test process, which are mainly divided into ignition, stable, and shutdown stages. It is proved that due to the insufficient combustion of kerosene and the low pressure of the combustion chamber at the initial stage of ignition, the flame discharged from the nozzle undergoes supplementary combustion, showing a feather-like expansion structure. This is a typical result of a short transition process in the early stage of ignition. In the stable working stage, the 4D C/C composite nozzle becomes bright red or even white when heated, and there are eight obvious diamond-shaped shock structures within the visible range of the image, which is consistent with the CFD simulation results. After the shutdown stage, the C/C nozzle cools down naturally and turns dark red. The results show that the composite material has withstood the test of high temperature supersonic flame, the auxiliary sealing of the specimen is complete, and the ablation test is successfully completed.

After the ablation test, the specimen is removed from the fixture and the ablation results are analyzed. Figure 15a shows the macroscopic morphology of the specimen after ablation, in which the throat is obviously eroded by the gas jet and particle flow. The errors of the ablation test mainly refers to the difference between the ablation rates (usually three different values) of the three samples after independent repeated tests. Since the absolute correct value of the ablation rate of the C/C composite under a certain ablation condition cannot be known in advance, the reference standard for error calculation is actually based on the average value obtained from three independent repeated tests (each specimen also needs to be measured several times). As shown in Figure 15b, the average line ablation rate is 0.053 mm/s, and the average mass ablation rate is 0.073 g/s in the ablation tests. The

errors of the parameters obtained by repeated experiments are lower than 4.72% and 6.15%, respectively. In the real flight condition, three complete nozzles of the same material are selected. Due to the slight differences on the material itself (density, etc.) and the working condition of the SRM in the three flight tests, there are also errors in the final ablation rate. The calculation methods of the error are the same as that of the ablation test, and the errors are essentially the deviation degree of the ablation rate from the mean value in independent samples. Moreover, the average line ablation rate and the mass ablation rate of the nozzle in the real flight condition are 0.066 mm/s and 0.091 g/s, whose errors are lower than 4.54% and 5.49%, respectively. The ablation rate of the actual flight is always slightly larger than that of the ablation test, which can be explained by the effect of the inevitable size and local oxidation effect. The size of the specimen used in the ablation test is about 8 mm, which has better heat dissipation performance because of its large specific surface area. Whereas the nozzle throat diameter of the actual engine can be up to 240 mm, which means the large-size specimen may have local non-uniform ablation phenomenon, resulting in a higher ablation rate than the ablation test. In addition, compared with the actual flight conditions, the fact that the propellant is burned more sufficiently in the ablation test reduces the unpredictable oxygen-rich region near the nozzle, thus reducing the possibility of C/C composites being oxidized, which also leads to the lower ablation rate obtained in the ablation test than the actual flight conditions. The phenomenon has also been observed in engine development institutions and relevant literatures [3,50]. Regardless, the ablative rate of the ground test is very close to that of the flight test, especially the absolute value difference which is very small, which proves that the ablation test system is reliable. Figure 15c–f are the microscopic SEM morphologies of the ablated specimens. Some fiber filaments are bare and the head is sharp, which is a typical chemical ablation, indicating that the material has an obvious tendency of preferentially ablation of the substrate. As shown in Figure 15c, the red area indicated by the arrow indicates that some molten Al₂O₃ spherical particles are solidified and deposited on the surface of the specimen during the ablation process. Meanwhile, Figure 15d shows the ablation morphology of similar parts after the flight test of the real SRM, where the matrix is also consumed first, and the fibers are obviously exposed. There are more debris and particles attached to the surface of the material, and the brighter irregular large particles are unmelted Al₂O₃ particles. The above results confirm that the mechanical erosion effect of the gas jet is also obvious in the process of the ablation.



The test results of the ablation morphology on the surface of the convergent section near the jet inlet direction are compared with the actual test flight results, as shown in Figure 15e,f. In the vertical direction, the specimen fibers are cylindrical and the matrix is ablated more easily than the fibers. The majority of the fiber tips are mechanically removed, resulting in normal fibers protruding in the matrix, the appearance of broken round heads, and even the formation of macroscopic pits. It can be seen that mechanical erosion mainly occurs at this position. Figure 15e shows that there are still a few sharp fibers, which is a typical phenomenon of chemical ablation.

In general, the ablation of C/C composites is a combination of chemical ablation and mechanical erosion. The chemical ablation mechanism of C/C composites is shown in the reaction equations below. The Al₂O₃ particles intensify the mechanical damage of the material mainly through mechanical collision, and changed the surface topography of the material, in-creased the reaction area and ablation effect [47,48]. The process of particle erosion is described by the theory of elastic-plastic indentation fracture. The fine particle erosion model reflects the process of fiber fracture and matrix damage by impact [11]. Mechanical erosion and chemical ablative processes interact with each other through the change of material morphology and physical and chemical properties, resulting in the final ablative results.

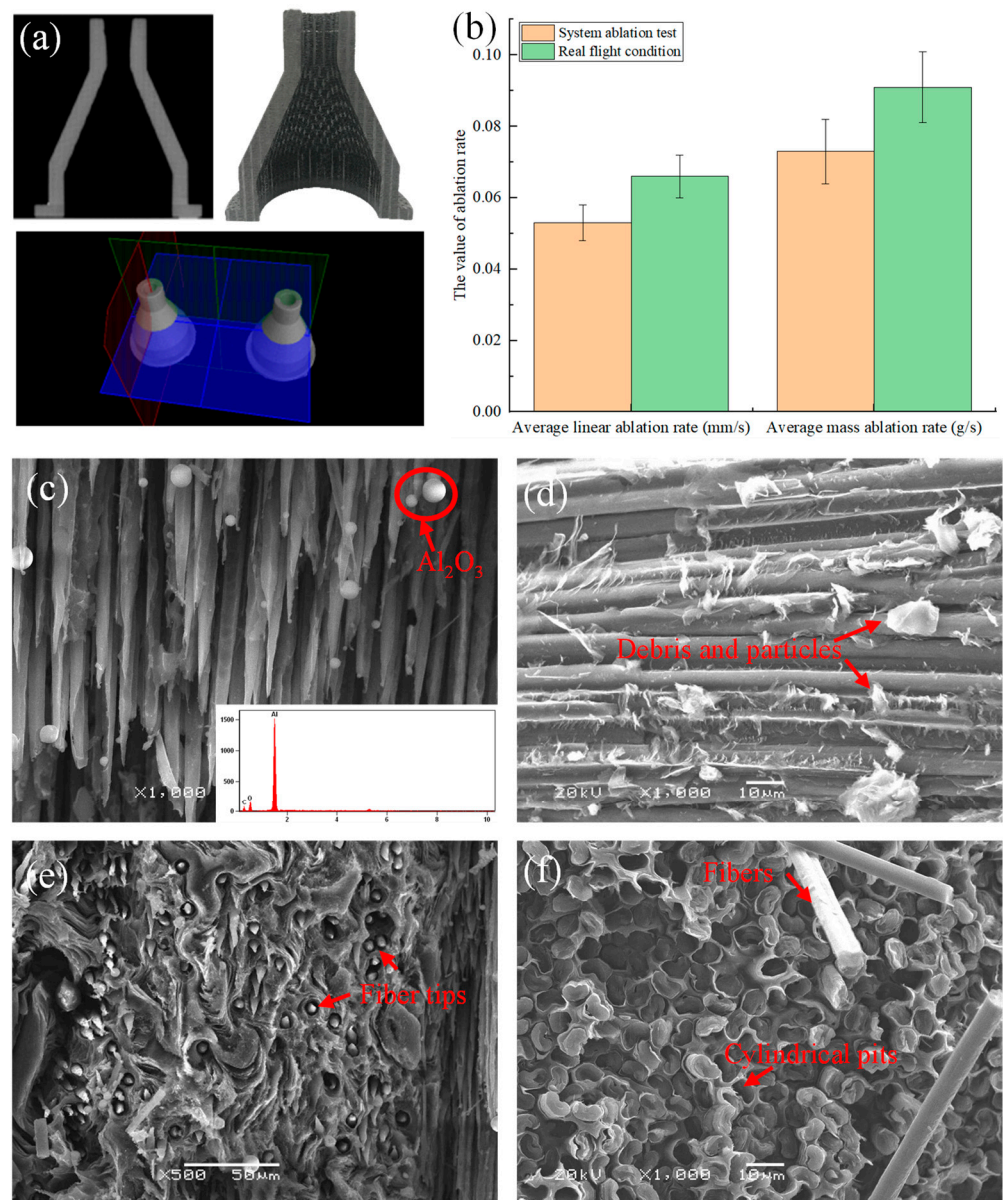


Figure 15. The morphology and ablation properties of C/C specimen: (a) Macroscopic ablation morphology; (b) Ablation rate in ablation test and real flight; fiber morphology along the depth of the substrate (c) in ablation test and (d) in the real flight test; micro ablation morphology close to the inlet of jet (e) in the ablation test and (f) in the real flight test.

The ablation test of the verification material shows that the ablation environment of this method is controllable, which is close to the real environment. In terms of the ablation mechanism, macroscopic and microscopic morphology are also relatively close.

The general applicability of the new ablation test method can be discussed in many aspects because of the LRE's characteristics of easy adjustment of the propellant flow and mixing ratio. Meanwhile, the particles can be conveniently selected and adjusted in different material and concentration ranges according to the needs of the multiphase flow. The ablation test system has great application value in the test of materials in various application environments (including ramjet and hypersonic vehicle, etc.). The following are some representative research areas. Case 1: The ablation test of insulation materials (usually silicone rubber material) in solid ramjet. B_2O_3 particles with similar properties to the solid ramjet fuel are used in the test. By adjusting the flow and mixing ratio of the propellant, the system can achieve a lower temperature and velocity, which shows that the

test system can well simulate the real engine operating environment. The specimen is still a typical Laval nozzle. Case 2: The ablation test of thermal protection materials (usually phenolic resin materials) on a rocket launch device. In the ablation test, the flow and mixing ratio of propellant can be adjusted, and the Al_2O_3 particles with the required concentration can be adjusted from 0 to 30%. In general, the specimen is a flat or a taper sample. This is an application based on an external flow field ablation test. Case 3: The hypersonic vehicle surface material (usually high temperature resistant ceramic or phenolic resin) ablation test. The test usually requires the production of a high temperature jet with a similar oxygen content and velocity to the incoming flow. At the same time, a small number of particles (small metal oxide particles or polyester material particles) in the ablation test can simulate the erosion of the hypersonic vehicle caused by dust impurities, ice crystals, and other harmful particles in the actual air flow. This is a kind of external field ablation test, and its typical application is the stagnation point ablation test of the head cone. In addition, as an extended application of the LRE system, the propellant can be replaced by LOX/LH₂ and LOX/methane, LOX/alcohol and so on, by properly improving the pressurization system and the atomization device. All of these changes depend on the more elaborate requirements of combustion products in the different ablation test tasks.

5. Conclusions

In this paper, a variable-precision general modular rocket engine system simulation method is proposed. Furthermore, a multiphase flow ablation test system based on the LRE and a particle delivery device is designed. It is proved that the method and the system can meet the requirements of the quantitative ablation test for some thermal protection materials by the unique internal flow field ablation test. The results show that the multidisciplinary dynamic system simulation method is helpful to design and analyze the test parameters more precisely, and the system has high feasibility and reliability. It is found that the 4D C/C composites have good ablation resistance and the ablative mechanism is similar to the actual flight test. The multi-dimensional simulation method reconciles the computational accuracy and speed of the simulation, and is of great value in the study of the dynamic characteristics of liquid rocket motor systems that focus on the details of other components. The main conclusions are as follows:

- (a) Based on the design of a gas-oxygen kerosene rocket engine, a multiphase flow ablation test system with adjustable particle concentration and propellant mixing ratio is developed by adding a high-pressure solid particle delivery device. Its unique internal flow field ablation operating temperature and pressure parameters range from 756 K to 3565 K and 0.2 to 4.2 MPa, respectively.
- (b) A multidisciplinary system simulation method of gas-oxygen kerosene rocket engine is proposed. Pipelines, valves, combustion chambers, pumps, and motors, are modeled through a modular graph modeling platform. Compared with the data of the sensors in the actual test, various simulation errors including pressure and temperature parameters are less than 5%, which can effectively guide the implementation of the test.
- (c) The co-simulation of the 3D CFD simulation of the combustion chamber and the 0D ablation test system model is completed by a variable precision system simulation method. The data exchange is completed through TCP/IP in a fixed time step, and the spatial distribution results of temperature, pressure, and velocity of the combustion chamber concerned by the test personnel are automatically given in real time. The CFD simulation results are consistent with the jet structure of the actual ignition test.
- (d) The internal multiphase flow ablation test is carried out on the 4D C/C composite specimens. The kerosene flow rate of 8.2 g/s and the oxygen flow rate of 24.6 g/s make the combustion chamber temperature reach 3380 K and the pressure is about 1 MPa. The line ablation rate of the specimen is 0.053 mm/s, and the mass ablation rate is 0.073 g/s, which are similar to the ablation results of the actual flight test. The C/C composite shows relatively good ablation resistance, and the ablation is the result

of the combined effect of thermochemical ablation and mechanical erosion of the multiphase flow.

Author Contributions: Conceptualization, Q.S. and B.Z.; funding acquisition, Z.S. and W.H.; validation, J.W., M.Y. and Z.S.; writing—original draft, Q.S.; writing—review and editing, M.Y. and Y.G. All authors have read and agreed to the published version of the manuscript.

Funding: This research was funded by the National Natural Science Foundation of China Major Research Program (No. 91952110) and the National Natural Science Foundation of China Joint Fund Project (No. U1737209).

Data Availability Statement: Not applicable.

Acknowledgments: The material analysis and testing work are supported by the State Key Laboratory of Tribology, Tsinghua University.

Conflicts of Interest: The authors declare no conflict of interest.

References

- Borrelli, R.; Riccio, A.; Tescione, D.; Gardi, R.; Marino, G. Thermo-structural behaviour of an UHTC made nose cap of a reentry vehicle. *Acta Astronaut.* **2009**, *65*, 442–456. [[CrossRef](#)]
- Squire, T.H.; Marschall, J. Material property requirements for analysis and design of UHTC components in hypersonic applications. *J. Eur. Ceram. Soc.* **2010**, *30*, 2239–2251. [[CrossRef](#)]
- Hui, W.; Bao, F.; Wei, X.; Liu, Y. Ablation performance of a 4D-braided C/C composite in a parameter-variable channel of a Laval nozzle in a solid rocket motor. *New Carbon Mater.* **2017**, *32*, 365–373. [[CrossRef](#)]
- Liu, L.; He, G.Q.; Wang, Y.H.; Hu, S.-Q.; Liu, Y.-M. Factors affecting the primary combustion products of boron-based fuel-rich propellants. *J. Propuls. Power* **2017**, *33*, 333–337. [[CrossRef](#)]
- Windhorst, T.; Blount, G. Carbon-carbon composites: A summary of recent developments and applications. *Mater. Des.* **1997**, *18*, 11–15. [[CrossRef](#)]
- Jin, X.; Fan, X.; Lu, C.; Wang, T. Advances in oxidation and ablation resistance of high and ultra-high temperature ceramics modified or coated carbon/carbon composites. *J. Eur. Ceram. Soc.* **2018**, *38*, 1–28. [[CrossRef](#)]
- Wang, R.; Li, N.; Zhang, J.; Liu, B.; Yan, N.; Fu, Q. Ablation behavior of sharp leading-edge C/C-ZrC-SiC composites using 3000 °C oxyacetylene torch. *Corros. Sci.* **2022**, *206*, 110551. [[CrossRef](#)]
- Zhuang, L.; Fu, Q.-G.; Tan, B.-Y.; Guo, Y.-A.; Ren, Q.-W.; Li, H.-J.; Li, B.; Zhang, J.-P. Ablation behaviour of C/C and C/C-ZrC-SiC composites with cone-shaped holes under an oxyacetylene flame. *Corros. Sci.* **2016**, *102*, 84–92. [[CrossRef](#)]
- Helber, B.; Chazot, O.; Magin, T.; Hubin, A. Ablation of carbon preform in the VKI Plasmatron. In Proceedings of the 43rd AIAA Thermophysics Conference, New Orleans, LA, USA, 25–28 June 2012; p. 2876.
- Chen, Y.; Li, H.; Sun, L.; Ren, M. Plasma ablation properties of C/C-Cu composites. *Acta Mater. Compos. Sin.* **2014**, *31*, 1238–1243.
- Liu, Y.; Li, X.C.; Li, J.; He, G.-Q.; Li, Z.-Y. Ablation model based on porous charring layer under alumina erosion condition. *AIAA J.* **2019**, *57*, 4792–4803. [[CrossRef](#)]
- Gao, Y.; Zha, B.L.; Wang, J.J.; Sun, Z.-S.; Zhang, Z.-F.; Shi, Y.-A. Ablation mechanism of C/C-SiC and C/C-SiC-ZrC composites in hypersonic oxygen-enriched environment. *Ceram. Int.* **2022**, *48*, 22985–22993. [[CrossRef](#)]
- Wei, X.; Yang, Z.; Zhu, S.; Zhao, Z.; Ye, J.; Haidn, O.J. The Confirmation of Thermal Boundary Parameters in an Oxygen Kerosene Fuel-Rich Rocket Engine. *Aerospace* **2022**, *9*, 343. [[CrossRef](#)]
- Tong, Y.; Bai, S.; Zhang, H.; Ye, Y. Laser ablation behavior and mechanism of C/SiC composite. *Ceram. Int.* **2013**, *39*, 6813–6820. [[CrossRef](#)]
- Liu, L.; Yang, L.; Zhao, C.; Xiao, X.; Ye, Z.; Zhang, J.; Wang, G.; Wang, Y. Oxide-scale evolution and dynamic oxidation mechanism of ZrB₂-SiC in high-enthalpy plasma wind tunnel. *J. Eur. Ceram. Soc.* **2021**, *41*, 3911–3921. [[CrossRef](#)]
- Yang, D.; Zhang, W.; Jiang, B.; Guo, Y. Silicone rubber ablative composites improved with zirconium carbide or zirconia. *Compos. Part A Appl. Sci. Manuf.* **2013**, *44*, 70–77. [[CrossRef](#)]
- Sutton, G.P. *History of Liquid Propellant Rocket Engines*; AIAA: Melbourne, FL, USA, 2006. [[CrossRef](#)]
- Zhang, Y.; Liu, K.; Cheng, M. *Dynamics Theory and Application of Liquid Rocket Motor*; Science Press: Beijing, China, 2005.
- Powell, M.; Butler, P.; Beck, L. Ground test simulation of rocket engine start transients. In Proceedings of the 11th Propulsion Conference, New Orleans, LA, USA, 19–21 March 1975; p. 1273.
- Meyer, C.; Maul, W. The application of neural networks to the SSME startup transient. In Proceedings of the 27th Joint Propulsion Conference, Sacramento, CA, USA, 24–26 June 1991; p. 2530.
- Goertz, C. A modular method for the analysis of liquid rocket engine cycles. In Proceedings of the 31st Joint Propulsion Conference and Exhibit, San Diego, CA, USA, 10–12 July 1995; p. 2966.
- Binder, M. An RL10A-3-3A rocket engine model using the Rocket Engine Transient Simulator (ROCETS) software. In Proceedings of the 29th Joint Propulsion Conference and Exhibit, Monterey, CA, USA, 28–30 June 1993; p. 2357.

23. Leudiere, V.; Albano, G.; Ordonneau, G.; Masse, J.; Legrand, B. CARINS: A versatile and flexible tool for engine transient prediction development status. In Proceedings of the 24th Symposium (International) on Technologies for Space, Tokyo, Japan, 24–25 September 2004.
24. Isselhorst, A. HM7B simulation with ESPSS tool on Ariane 5 ESC-A Upper Stage. In Proceedings of the 46th AIAA/ASME/SAE/ASEE Joint Propulsion Conference & Exhibit, Nashville, TN, USA, 25–28 July 2010; p. 7047.
25. Fan, Z.; Huang, M.; Yu, Y. Modular Model of Space Propulsion System in the Whole Operation Process. *J. Natl. Univ. Def. Technol.* **2007**, *29*, 29–33.
26. Zhang, L.; Li, W.; Duan, N. Modular general simulation of liquid rocket motor. *J. Aerosp. Power* **2011**, *26*, 687–691.
27. Wang, C.; Zhang, X.; Gao, Y.; Chen, H. Research on the acceleration spin-up scheme of oxygen pre-pressure pump during the starting process of liquid oxygen kerosene supplemented combustion engine. *Propuls. Technol.* **2020**, *41*, 8. [[CrossRef](#)]
28. Chen, H.; Liu, H.; Chen, J. Forced start process of supplementary combustion cycle engine. *J. Aerosp. Power* **2015**, *30*, 3010–3016. [[CrossRef](#)]
29. Pan, H.; Zhang, L. Application of AMESim software in dynamic simulation of liquid rocket engine system. *Rocket. Propuls.* **2011**, *37*, 6–11. [[CrossRef](#)]
30. Li, J. A fast method for dynamic simulation of low temperature engine system. *Missile Space Launch Technol.* **2012**, *1*, 13–17. [[CrossRef](#)]
31. Zheng, D.; Wang, H.; Hu, J. Research on transient characteristics of high-thrust hydrogen-oxygen engine. *Propuls. Technol.* **2021**, *42*, 1761–1769. [[CrossRef](#)]
32. Liu, Y.; Fu, B.; Yang, J.; He, G.; He, Y.; Liu, P. Modeling and simulation of electric pump-pressure liquid rocket engine system. *Manned Aerosp.* **2019**, *25*, 107–115. [[CrossRef](#)]
33. Cui, P.; Song, J.; Li, Q.; Chen, L.; Liang, T.; Sun, J. Dynamics modeling and simulation analysis of electric pump-pressure liquid Kerosene Variable Thrust Rocket Engine: Part I-Single-Point Condition Analysis. *Chin. J. Aeronaut. Astronaut.* **2022**, *43*, 248–262. [[CrossRef](#)]
34. Wang, Z. *Design of Thrust Chamber for Liquid Rocket Motor*; National Defense Industry Press: Beijing, China, 2014.
35. Cao, T. *Rocket Engine Dynamics*; National University of Defense Technology Press: Beijing, China, 2004.
36. Zhai, Y. *Research on Dynamic Simulation of Expansion Cycle Engine Thrust Regulation Process*; China Aerospace Science and Technology Corporation: Beijing, China, 2017.
37. Glickman. *Automatic Adjustment of Liquid Rocket Motor Translated by Gu Mingchu*; Aerospace Press: Beijing, China, 1995.
38. Siemens. *Simcenter AMESim 2021.1 Thermal Hydraulic Component Design Library User's Guide*; Siemens Industry Software NV: Plano, TX, USA, 2021.
39. Siemens. *Simcenter AMESim 2021.1 Pneumatic Library User's Guide*; Siemens Industry Software NV: Plano, TX, USA, 2021.
40. Siemens. *Simcenter AMESim 2021.1 Signal, Control Library User's Guide*; Siemens Industry Software NV: Plano, TX, USA, 2021.
41. Siemens. *Simcenter AMESim 2021.1 Gas Mixture Library User's Guide*; Siemens Industry Software NV: Plano, TX, USA, 2021.
42. Stark, R.H. Flow separation in rocket nozzles—an overview. In Proceedings of the 49th AIAA/ASME/SAE/ASEE Joint Propulsion Conference, San Jose, CA, USA, 14–17 July 2013; p. 3840.
43. Siemens. *Simcenter AMESim 2021.1 Thermal Library User's Guide*; Siemens Industry Software NV: Plano, TX, USA, 2021.
44. Siemens. *Simcenter AMESim 2021.1 Electrical Basics Library User's Guide*; Siemens Industry Software NV: Plano, TX, USA, 2021.
45. Siemens. *Simcenter AMESim 2021.1 Electric Motors and Drives library User's Guide*; Siemens Industry Software NV: Plano, TX, USA, 2021.
46. Munson, B.R.; Okiishi, T.H.; Huebsch, W.W.; Rothmayer, A.P. *Fluid Mechanics*; Wiley: Singapore, 2013.
47. Deng, W. *Numerical Study of Particle Erosion in Solid Rocket Motor Nozzle*; Harbin Engineering University: Harbin, China, 2017.
48. Zhang, S.; Hu, C.; Xu, Y.; Chen, J. Combustion characteristic analysis on condensed-phase particle in SRM chamber. *J. Solid Rocket Technol.* **2010**, *33*, 256–259. [[CrossRef](#)]
49. Zhang, S.; Hu, C.; Xia, S.; Li, J. Experimental investigation on the condensed particles size distribution at srm nozzle throat. *J. Propuls. Technol.* **2012**, *32*, 245–248. [[CrossRef](#)]
50. Wang, H.; Li, X. Multiscale approach to ablation modeling of in-plain C/C composite for nozzle throat. *J. Solid Rocket Technol.* **2017**, *3*, 295–301.